Non-linear aeroelastic behavior of large horizontal-axis wind turbines

A multibody system approach

Gebhardt, C. G. ; Preidikman, S.; Jørgensen, Martin Heide; Massaa, J.C.

Published in:
International Journal of Hydrogen Energy

DOI (link to publication from Publisher):
10.1016/j.ijhydene.2011.12.090

Publication date:
2012

Document Version
Early version, also known as pre-print

NON-LINEAR AEROELASTIC BEHAVIOR OF LARGE HORIZONTAL AXIS WIND TURBINES: A MULTIBODY SYSTEM APPROACH

Gebhardt C.G. [1,3] , Preidikman S [1,3] , Jørgensen M.H.[2] and Massa J.C. [1]

(1) Structures Department, National University of Cordoba, Av. Vélez Sarsfield 1611, Casilla de Correo 916, 5000 Córdoba, Argentina
(2) Department of Mechanical and Manufacturing Engineering, Aalborg University, Fibigerstræde 16, 9220 Aalborg east, Denmark.
(3) CONICET, Av. Rivadavia 1917, 1033 Buenos Aires, Argentina.
e-mail: cgebhardt@efn.uncor.edu

ABSTRACT

This paper shows the development of a flexible multibody model, which coupled with an existing aerodynamical model, is used to numerically simulate the non-linear aeroelastic behavior of large horizontal axis wind turbines. The model is rather general; different configurations could be easily simulated and it is primarily intended to be used as a research tool to investigate influences of detailed dynamic effects. It includes: *i*) a supporting tower; *ii*) a nacelle which contains the electrical generator, the power electronics and the control systems; *iii*) a hub where the blades are attached and connected to the generator rotating shaft; and, *iv*) three blades which extract energy from the airstream.

The blades are considered flexible, and their equations of motion are discretized in the space domain by using beam finite elements capable of taking into account the non-linearities coming from the kinematics. The tower is also considered flexible, but its equations of motion are discretized by using the method of assumed-modes. The nacelle and hub are considered rigid, and are represented by taking into account the effects of the kinematical non-linearities.

Due to the system complexity, the tower, nacelle and hub are modeled as a single kinematical chain and each blade is modeled separately. Constraint equations are used to connect the blades to the hub. The governing equations are differential-algebraic since ordinary differential equations and algebraic constraint equations are involved, due to the presence of rigid and discretized flexible bodies and linkage among bodies, respectively. All the equations are solved numerically and interactively in the time domain by using a fourth-order predictor-corrector scheme.

Key words: wind turbines, rigid-flexible multibody systems, aerodynamic loads, aeroelastic behavior.

1. INTRODUCTION

During the last two decades, due to the necessity to obtain clean sources of energy, the interest in designing wind turbines increasingly large has been growing. To obtain efficient designs, it is necessary to develop precise and robust techniques able to predict the aeroelastic characteristics of such systems. Across the years, aiming at this target, several authors have been developed structural models to study the dynamical behavior of large horizontal-axis wind turbines (LHAWT) and very different approaches have been explored.

Petersen [1] presented a time domain model for simulating the dynamic response of a horizontal axis wind turbine. A general kinematic analysis was used to derive the local inertial loads. The wind turbine is subdivided into three sub-structures: the tower, the nacelle-shaft and the rotor blade. The model is discretized using the finite element technique. Lee et al. [2] developed a methodology representing the wind turbine as a multi-flexible-body system with both rigid and flexible body sub-systems. Rigid body sub-systems (nacelle, hub) are modeled using Kane's method, and flexible body sub-systems (tower, blades), using geometrically exact, non-linear beam finite elements. Jonkman and Buhl [3] developed the FAST code which is a comprehensive aeroelastic simulator. The FAST model employs a combined modal and multi-body dynamics formulation. Blades and tower are characterized using a linear modal representation while the remaining components are modeled as rigid bodies. Zhao et al. [4] developed a methodology based on the hybrid multi-body system composed of rigid, flexible bodies, force elements and joints. With a cardanic joint beam element, the flexible bodies are modeled as

sets of rigid bodies connected by cardanic joints; thus a whole wind turbine structure can be represented by a discrete system of rigid bodies, springs, and dampers. A very detailed study focused on the rotor blade was developed by Kallesøe [5], who proposed an extension of Hodges-Dowell's partial differential equations of blade motion [6], by including the effects of gravity, pitch action and rotor speed variations. The partial differential equations of motion are approximated by ordinary differential equations (ODEs) of motion using an assumed-modes method.

This paper presents a reduced order structural model of a three-blade LHAWT. The blades are considered flexible, and their equations of motion (EoMs) are discretized in the space domain by using beam finite elements capable of taking into account the non-linearities coming from the kinematics. The tower is also considered flexible, but its EoMs are discretized using the method of assumed-modes. The nacelle and hub are considered rigid, and are represented by a geometric formulation which allows taking into account the effects of the kinematical non-linearities [7,8]. The current model involves different modeling approaches; in addition, the combination of different techniques for modeling the LHAWT components renders a very precise reduced order model. For solving the LHAWT EoMs in the time domain, a scheme based on a modified version of the fourth order Hamming's predictor-corrector method is used [9].

2. DYNAMICAL MODEL

2.1 Tower, Nacelle and Hub

In this work, the tower, nacelle and hub are considered members of a single kinematical chain. It means that the position and orientation of any given point belonging to nacelle is related to the tower and the position and orientation of any given point belonging to the hub is related to the nacelle.

The tower is modeled as a straight prismatic, linearly elastic, undamped beam. The root of the tower is rigidly attached to the ground and the nacelle is mounted at the top. The assumed-modes method [10,11] is used to obtain a model for the tower with few degrees of freedom (DoFs). We considered a mode for the after-forward bending, a mode for the side-to-side bending and another one for torsion about the longitudinal axis.

The nacelle and hub are modeled as rigid bodies. The nacelle can rotate respect to the tower in a yaw angle, which is commanded by the control system. The hub can freely rotate respect to the nacelle in an azimuth angle. Both rotations are represented by a sequence of Euler's angles.

The EoMs for the tower, nacelle and hub as a single kinematical chain can be expressed as

$$[\mathbf{M}_{tnh}]\{\ddot{\mathbf{q}}_{tnh}\}+[\mathbf{K}_{tnh}]\{\mathbf{q}_{tnh}\}=\{\mathbf{f}^{g}_{tnh}+\mathbf{f}^{k}_{tnh}+\mathbf{f}^{c}_{tnh}\}, \quad (1)$$

where $\mathbf{q}_{tnh}$ is the vector of generalized coordinates, $\mathbf{M}_{tnh}$ and $\mathbf{K}_{tnh}$ are the mass and stiffness matrices, respectively. $\mathbf{f}^{g}_{tnh}$ is the vector of generalized forces accounting the contributions coming from the aerodynamics, the gravitational field, the control systems and the electrical generator. $\mathbf{f}^{k}_{tnh}$ is a vector of kinematical forces accounting for the centrifugal and Coriolis' effects on the nacelle and hub and $\mathbf{f}^{c}_{tnh}$ is the constraint forces vector due to effects of the blades, which is computed as

$$\{\mathbf{f}^{c}_{tnh}\} = -\sum_{i=1}^{3}\left[\frac{\partial \boldsymbol{\phi}_i}{\partial \mathbf{q}_{tnh}}\right]^{T}\{\boldsymbol{\lambda}_i\}, \quad (2)$$

where $\boldsymbol{\phi}_i$ is the set of constraint equations corresponding to the *i*-th blade and $\boldsymbol{\lambda}_i$ is its vector of Lagrange's multipliers [12, 13].

2.2 Blades

Each blade is modeled as a non-straight, linearly elastic, undamped beam. We consider, separately, large displacements and rotations due to motions of the blade as a rigid body, and small displacements and rotations due to the elastic deformation. The motions of the blade as a rigid body are called *primary motions* and its elastic motions are called *secondary motions*.

The *primary motions* give the position and orientation of the blades. The position is described by using three generalized coordinates and the orientation, by a unit quaternion [8,12], i.e. four generalized coordinates constrained because the addition of their squares must be always equal to 1.

The *secondary motions* leads us to a set of partial differential equations for a continuous elastic medium. To obtain a finite set of ODEs, the blades are discretized using two-node beam finite elements along the elastic axis, where each node has six DoFs. In this work the structural mesh of the blade has twenty-two nodes.

The EoMs for *primary motions* of blade 1 can be expressed as

$$[\boldsymbol{\mathcal{M}}_1]\{\ddot{\mathbf{q}}_1\}+[\boldsymbol{\mathfrak{M}}_1]\{\ddot{\mathbf{p}}_1\}=\{\boldsymbol{f}^{g}_{1}+\boldsymbol{f}^{k}_{1}+\boldsymbol{f}^{c}_{1}\}, \quad (3)$$

where $\mathbf{q}_1$ and $\mathbf{p}_1$ are the generalized coordinates for *primary* and *secondary motions*, respectively. $\boldsymbol{\mathcal{M}}_1$ is the mass matrix for *primary motions* and $\boldsymbol{\mathfrak{M}}_1$ is the mass matrix which couples the *primary* and *secondary motions*. $\boldsymbol{f}^{g}_{1}$ and $\boldsymbol{f}^{k}_{1}$ are vectors accounting for the generalized and kinematical forces, respectively, and $\boldsymbol{f}^{c}_{1}$ is the constraint forces vector due to the blade-hub attachment, which is computed as

$$\left\{ f_1^c \right\} = -\left[\frac{\partial \boldsymbol{\phi}_1}{\partial \mathbf{q}_1} \right]^T \left\{ \boldsymbol{\lambda}_1 \right\}. \quad (4)$$

The EoMs for *secondary motions* of blade 1 can be expressed as

$$[\mathbf{M}_1]\{\ddot{\mathbf{p}}_1\} + [\mathfrak{M}_1]^T \{\ddot{\mathbf{q}}_1\} + [\mathbf{K}_1]\{\mathbf{p}_1\} = \{\mathbf{f}_1^g + \mathbf{f}_1^k\}, \quad (5)$$

where $\mathbf{M}_1$ and $\mathbf{K}_1$ are the mass and stiffness matrices, and $\mathbf{f}_1^g$ and $\mathbf{f}_1^k$ are vectors accounting for the generalized and kinematical forces, respectively. These EoMs are reduced in size at every time step by using a modal projection scheme. The EoMs of blades 2 and 3 are obtained using a similar procedure.

2.3 Constraints

The roots of the blades are attached to the hub. Each blade can rotate respect to the hub in a pitch angle, which is commanded by the control system. Six constraint equations establish the linkage between the hub and each blade, three of them to specify the position and the other three to specify the orientation. An extra constraint equation is required to specify the unit quaternion condition.

The set of algebraic constraint equations for blade 1 can be expressed as [12, 13]

$$\boldsymbol{\phi}_1 \left(\mathbf{q}_{tnh}, \mathbf{q}_1 \right) = \mathbf{0}, \quad (6)$$

where only holonomic constraints are considered.

Constraint equations for blades 2 and 3 are obtained following the same procedure.

2.4 Governing equations

The governing equations for the whole system are differential-algebraic equations (DAEs) since ODEs and algebraic constraint equations are involved. After deriving the constraint equations twice respect to time, the governing equations can be expressed as

$$\begin{bmatrix} \mathbf{M} & \mathbf{B}^T \\ \mathbf{B} & \mathbf{0} \end{bmatrix} \begin{Bmatrix} \ddot{\mathbf{x}} \\ \boldsymbol{\lambda} \end{Bmatrix} = \begin{Bmatrix} \mathbf{f} \\ -\dot{\mathbf{B}}\dot{\mathbf{x}} \end{Bmatrix}, \quad (7)$$

where $\mathbf{f}$ is a force vector containing all the contributions explained in previous subsections,

$$[\mathbf{M}] = \begin{bmatrix} \mathbf{M}_{tnh} & \mathbf{0} & \mathbf{0} & \mathbf{0} & \mathbf{0} & \mathbf{0} & \mathbf{0} \\ \mathbf{0} & \mathcal{M}_1 & \mathfrak{M}_1 & \mathbf{0} & \mathbf{0} & \mathbf{0} & \mathbf{0} \\ \mathbf{0} & \mathfrak{M}_1^T & \mathbf{M}_1 & \mathbf{0} & \mathbf{0} & \mathbf{0} & \mathbf{0} \\ \mathbf{0} & \mathbf{0} & \mathbf{0} & \mathcal{M}_2 & \mathfrak{M}_2 & \mathbf{0} & \mathbf{0} \\ \mathbf{0} & \mathbf{0} & \mathbf{0} & \mathfrak{M}_2^T & \mathbf{M}_2 & \mathbf{0} & \mathbf{0} \\ \mathbf{0} & \mathbf{0} & \mathbf{0} & \mathbf{0} & \mathbf{0} & \mathcal{M}_3 & \mathfrak{M}_3 \\ \mathbf{0} & \mathbf{0} & \mathbf{0} & \mathbf{0} & \mathbf{0} & \mathfrak{M}_3^T & \mathbf{M}_3 \end{bmatrix} \quad (8)$$

is the system mass matrix,

$$[\mathbf{B}] = \begin{bmatrix} \frac{\partial \boldsymbol{\phi}_1}{\partial \mathbf{q}_{tnh}} & \frac{\partial \boldsymbol{\phi}_1}{\partial \mathbf{q}_1} & \mathbf{0} & \mathbf{0} & \mathbf{0} & \mathbf{0} & \mathbf{0} \\ \frac{\partial \boldsymbol{\phi}_2}{\partial \mathbf{q}_{tnh}} & \mathbf{0} & \mathbf{0} & \frac{\partial \boldsymbol{\phi}_2}{\partial \mathbf{q}_2} & \mathbf{0} & \mathbf{0} & \mathbf{0} \\ \frac{\partial \boldsymbol{\phi}_3}{\partial \mathbf{q}_{tnh}} & \mathbf{0} & \mathbf{0} & \mathbf{0} & \mathbf{0} & \frac{\partial \boldsymbol{\phi}_3}{\partial \mathbf{q}_3} & \mathbf{0} \end{bmatrix} \quad (9)$$

is the system constraint jacobian matrix,

$$\mathbf{x} = \left\{ \mathbf{q}_{tnh} \;\; \mathbf{q}_1 \;\; \mathbf{p}_1 \;\; \mathbf{q}_2 \;\; \mathbf{p}_2 \;\; \mathbf{q}_3 \;\; \mathbf{p}_3 \right\}^T \quad (10)$$

is the generalized coordinates vector, and

$$\boldsymbol{\lambda} = \left\{ \boldsymbol{\lambda}_1 \;\; \boldsymbol{\lambda}_2 \;\; \boldsymbol{\lambda}_3 \right\}^T \quad (11)$$

is the Lagrange's multipliers vector

3. AERODYNAMIC LOADS

Let us consider a body immersed in a fluid stream. When the Reynold's number is large, the viscous effects can be confined to those regions close to the solid surface; these vorticity-dominated regions are called boundary layers. Part of the vorticity contained in the boundary layers is shed downstream into the flow field, where it can only be transported by the fluid particles, but neither created nor destroyed. This transported vorticity forms the wakes behind the body.

The thickness of the boundary layers and wakes tends to zero when the Reynold's number tends to infinity. Under this condition, the boundary layers and wakes can be represented as continuous bounded and free sheets of vorticity, respectively.

In the Unsteady Vortex-Lattice Method (UVLM), the continuous bounded vortex sheets of the boundary layers are discretized into a lattice of short, straight vortex segments of constant circulation. These segments divide the surface of the body into a finite number of area elements. The model is completed by joining free vortex lines, representing the continuous free vortex sheets of the wakes, to the bounded vortex lattice along the separation sharp edges where the separation takes place. In our study case the separation edges are the trailing edges and tips of the rotor blades.

Each area element in the lattice is enclosed by a loop of vortex segments. To reduce the size of the problem, each element is considered to be enclosed by a closed loop of vortex segments having the same circulation, i.e. vortex rings of constant circulation. Then the spatial conservation of circulation is automatically satisfied.

The circulations of the vortex rings are determined by using a discrete version of the non-penetration boundary condition, the fluid cannot penetrate the solid surface, taking into account the contribution

of the free stream, the wakes and the velocity of the solid surface. At each step of time, after the determination of the rings circulations, vortex segments are shed into the flow-field and become part of the grids that approximate the free vortex sheets of the wakes.

By using an extended version of the UVLM developed by Gebhardt et al. [14], we estimate the magnitude and evolution of the aerodynamic loads in the time domain. This version allows taking into account the presence of both, the tower and the land-surface boundary layer. The capability to capture these phenomena is a novel aspect of the aerodynamical model.

4. NUMERICAL INTEGRATION SCHEME

The second-order governing differential equations have to be re-written as first order system and integrated in the time domain as follows:

1. At $t = 0$ the initial conditions are known.
2. At $t = \Delta t$ the solution is predicted by the explicit Euler's method, and then corrected iteratively by the modified Euler's method.
3. At $t = 2\Delta t$ the solution is predicted by the two-step Adams-Bashfort method, and then corrected iteratively by the two-steps Adams-Moulton method.
4. At $t = 3\Delta t$ the solution is predicted by the three-step Adams-Bashfort method, and then corrected iteratively by the three-step Adams-Moulton method.
5. At $t = n\Delta t$, for $n \geq 4$ the solution is predicted and corrected by the fourth order modified Hamming's method [9].

It is important to remark that, Lagrange's multiplier values are obtained at every time step as part of the solution.

Due to the constraints, this kind of systems usually shows some instabilities which can be easily suppressed by using the Baumgarte's stabilization scheme [15].

This integration methodology allows solving problems in which acceleration terms are present on both sides of the governing equations. This is a requirement since the aerodynamic loads depend on acceleration, velocity, position and orientation of the blades, and the estimation of these forces must be carried out at integer multiples of the time steps. In general the aerodynamic loads computation represents the highest computing cost, and its evaluation inside the time steps would be very expensive.

5. RESULTS

This section presents the results obtained with the computational tool based on the developed model. Simulations were carried out for a standard 3-blade LHAWT with 45-meter blades and a 68-meter tower, which is erected in a flat terrain with very low building density as any rural zone. The structural model has a total of 13 DoFs, which includes 3 for the tower, 1 for the rotor and 3 for each blade.

In the present effort, the cases of study focus on the response of the LHAWT under different wind conditions and keeping the yaw and pitch configurations fixed. To reach this goal we consider two different wind speeds, 15 and 20 m/s, at which the responses of the tower, rotor and blades are investigated. It is important to remark that these are reference values for the land-surface boundary layer, since the wind profile is not constant but rather varies with height.

4.1 Case v_{wind} = 15 m/s

In Figure 1, the rotor angular speed is plotted as a function of revolutions. The rotor speed increases gradually until it reaches the steady state after two and half revolutions. This is due to the power rate of the electrical generator and the aerodynamic damping. In the steady state, the angular speed is approximately 7.4 RPM and the mean produced power is 1.2 MW.

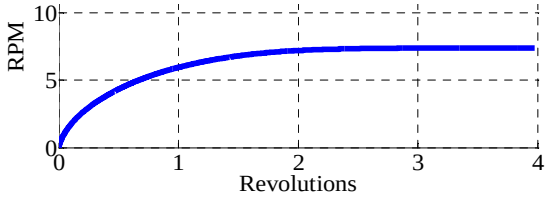

Figure 1. Rotor angular velocity.

In Figure 2, the after-forward displacement of the tower top is plotted. The tower bends forward and vibrates respect to an equilibrium position with small amplitude. This behavior is dominated by the gravitational loads due to the heavy masses of the hub, the nacelle and blades positioned in front of the tower. These actions predominate on the aerodynamic loads which push the tower backwards.

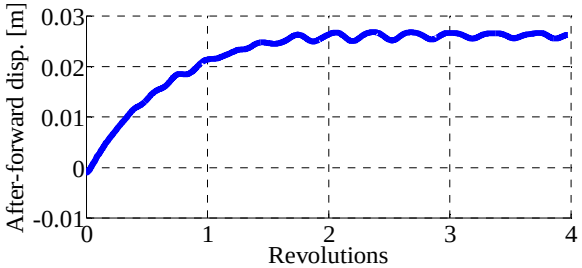

Figure 2. After-forward displacement of the tower.

In figure 3, the side-to-side displacement of the tower top is plotted. The tower bends to the left because the electrical generator produces a reacting moment when it takes energy from the rotor (power rate) which rotates clock-wise. The tower vibrates respect an equilibrium position, but the amplitude is higher than the after-forward displacement.

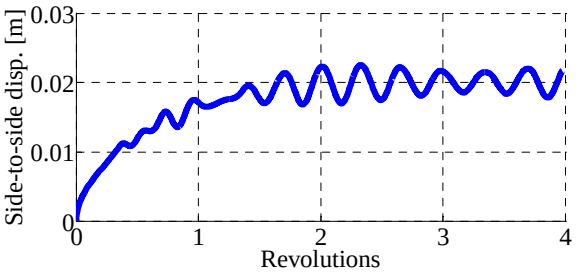

Figure 3. Side-to-side displacement of the tower.

In Figure 4, the flap-wise displacements of the blade tips are plotted. The blades bend up and vibrate; the mean value depends on the aerodynamic loads but the amplitude of the vibration is mainly governed by the gravitational loads. It is very important to remark that the responses of the blades present a dephasing angle of 120° that shows coherence respect to the geometric configuration of the rotor.

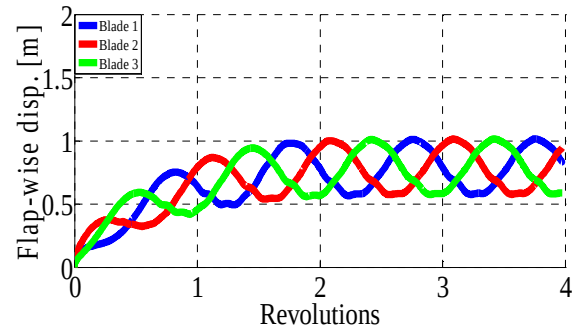

Figura 4. Flap-wise displacement of the blades.

In Figure 5, the edge-wise displacements of the blades tips are plotted. The blades vibrate in the edge direction with a mean value close to the undeformed position, because the gravitational forces predominate, and so when the blades are climbing or falling, they encounter almost the same load distribution but the sign changes.

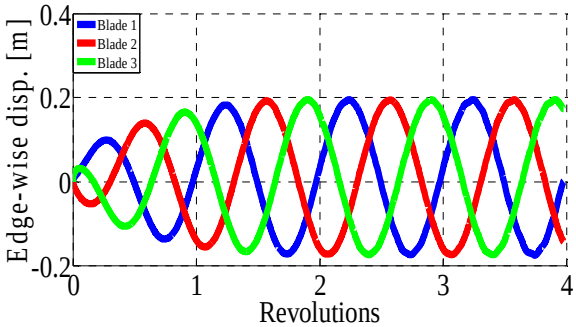

Figura 5. Edge-wise displacement of the blades.

4.2 Case v_{wind} = 20 m/s:

In Figure 6, the rotor angular speed is plotted. The rotor speed shows the same trend of the previous case but in the steady state, the angular speed is approximately 11.5 RPM and the mean produced power is 2.9 MW. Despite the 33% increase in wind speed, the angular speed and mean produced power increase 55% and 142%, respectively. This fact shows the non-linear characteristic of the attacked problem.

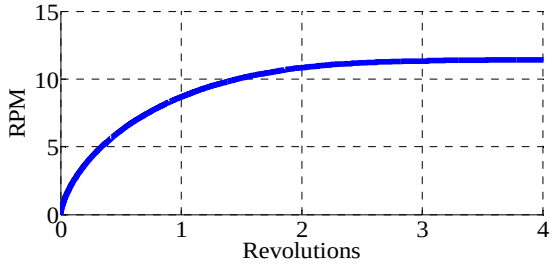

Figure 6. Rotor angular velocity.

In Figure 7, the after-forward displacement of the tower top is plotted. The tower bends backwards and returns close to the undeformed position. From this position, the tower vibrates with small amplitude because at the beginning the aerodynamic loads predominate but after some time only gravitational loads do. Note that this behavior is different from the one observed in Figure 2.

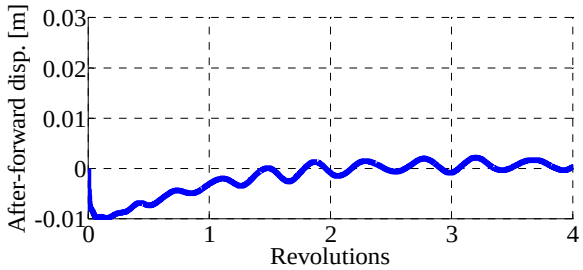

Figure 7. After-forward displacement of the tower.

In Figure 8, the side-to-side displacement of the tower top is plotted. As in the previous case, the tower bends to the left but this time the mean value and amplitude increase 50% and 200%, respectively.

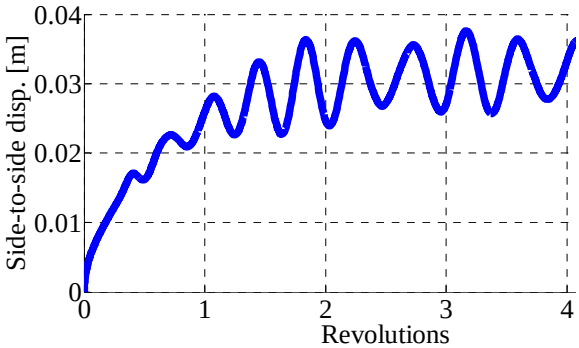

Figure 8. Side-to-side displacement of the tower.

In Figure 9, the flap-wise displacements of the blade tips are plotted. As in the previous case, the blades bend up showing the same trend, but the mean value increases 67% whereas the amplitude does changes significantly.

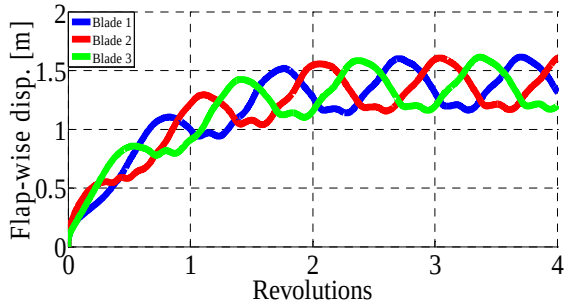

Figura 9. Flap-wise displacement of the blades.

In Figure 10, the edge-wise displacements of the blades tips are plotted. As in the previous case, the blades vibrate. Although the mean value and the amplitude increase a little, changes are no relevant since the gravitational forces predominate.

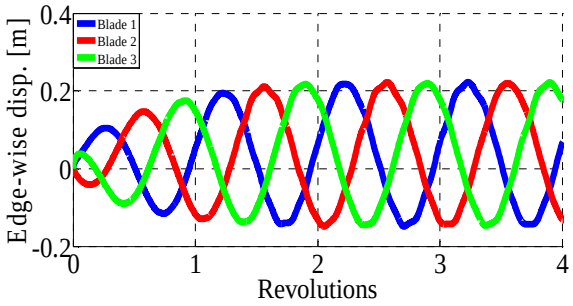

Figura 10. Edge-wise displacement of the blades.

6. CONCLUDING REMARKS

It can be concluded that, as the wind speed increases, the steady state angular speed and the produced power also increase. However, the second grows faster and shows a strong non-linearity.

The after-forward displacement of the tower strongly depends on the gravitational loads when the wind speed is not very large, but as the wind speed increases the aerodynamic loads become more and more relevant.

The side-to-side displacement of the tower depends on the aerodynamic loads and the power rate of the electrical generator.

The mean value of the flap-wise displacement mainly depends on the aerodynamic loads. However, the amplitude of the vibrations mainly depends on the gravitational loads.

The edge-wise displacement mainly depends on the gravitational loads and it does not change significantly when the wind speed varies.

Although the proposed model constitutes a good starting point to get an understanding of the aeroelastic behavior of LHAWTs, in the future it will be necessary to expand the present ideas and add a very precise model of the power generation dynamics, the dynamics of the electrical network and/or the dynamics associated to a hydrogen production system based on wind energy.

7. REFERENCES

[1] Petersen J.T., "Kinematically non-linear finite element model of a horizontal-axis wind turbine", Ph.D. Thesis, Risø National Laboratory, 1990.

[2] Lee D.L., Hodges D.H., Patil M.J. "Multi-flexible-body dynamic analysis of horizontal-axis wind turbines", Wind Energy **5**, 2002, pp. 281-300.

[3] Jonkman J.M. and Buhl M.L. Jr., "FAST user's guide", Technical Report NREL/EL-500-38230, NREL, 2005.

[4] Zhao X., Maiβer P. and Wu J., "A new multi-body modeling methodology for wind turbine structures using a cardanic joint beam element", Renewable Energy **32**, 2007, pp. 532-546.

[5] Kallesøe B.S., "Equations of motion for a rotor blade, including gravity, pitch action and rotor speed variations", Wind Energy **10**, 2007, pp. 209-203.

[6] Hodges D.H. and Dowell E.H., "Nonlinear equations of motion for the elastic bending and torsion of twisted nonuniform rotor blades", Technical Report TN D-7818, NASA, 1974.

[7] Maiβer P., "Analytical dynamics of multi-body systems", Computer Methods in Applied Mechanics and Engineering **91**, 1991, pp. 1391-1396.

[8] Heard W.B., "Rigid Body Mechanics: Mathematics, Physics and Applications", Wiley, 2006.

[9] Preidikman S., "Numerical simulation of interactions among aerodynamics, structural dynamics, and control systems", Ph.D. Thesis, Virginia Polytechnic Institute, 1998.

[10] Meirovith L., "Computational Methods in Structural Dynamics", Springer, 1980.

[11] Kane T.R., Ryan R.R. and Banerjee A.K., "Dynamics of a cantilever beam attached to a moving base", Journal of Control and Guidance **10**, 1987, pp. 139-151.

[12] Nikravesh P.E., "Computer-Aided Analysis of Mechanical Systems", Prentice-Hall, 1988.

[13] Shabana A.A., "Dynamics of Multibody Systems", Cambridge University Press, 2010.

[14] Gebhardt C., Preidikman S. and Massa J., "Numerical simulations of the aerodynamic behavior of large horizontal-axis wind turbines", International Journal of Hydrogen Energy **35**, 2010, pp. 6005-6011.

[15] Baumgarte J., "Stabilization of Constrains and Integrals of Motion in Dynamical Systems", Computer Methods in Applied Mechanics and Engineering **1**, 1972, pp. 1-16.